AIP Advances

RESEARCH ARTICLE | NOVEMBER 09 2022

# First-principles quantum treatment of electron–phonon interactions in thin-film nanodevices

Md. Samzid Bin Hafiz ; Quazi Deen Mohd Khosru; Momotaz Begum; Bimal Chandra Das



*AIP Advances* 12, 115015 (2022)
https://doi.org/10.1063/5.0124158

# First-principles quantum treatment of electron–phonon interactions in thin-film nanodevices

Cite as: AIP Advances 12, 115015 (2022); doi: 10.1063/5.0124158
Submitted: 3 September 2022 • Accepted: 15 October 2022 •
Published Online: 9 November 2022



Md. Samzid Bin Hafiz,[1,a)] Quazi Deen Mohd Khosru,[2] Momotaz Begum,[3] and Bimal Chandra Das[4]

## AFFILIATIONS

[1]Department of Electrical and Electronic Engineering, Dhaka University of Engineering and Technology, Gazipur, Bangladesh
[2]Department of Electrical and Electronic Engineering, Bangladesh University of Engineering and Technology, Dhaka, Bangladesh
[3]Department of Computer Science and Engineering, Dhaka University of Engineering and Technology, Gazipur, Bangladesh
[4]Daffodil International University, Dhaka, Bangladesh

[a)]**Author to whom correspondence should be addressed:** samzid.eee@duet.ac.bd

## ABSTRACT

Electron–phonon interactions play a crucial role in nano-electronic device performance. As the accurate calculation of these interactions requires huge computational resources, reduction of this burden without losing accuracy poses an important challenge. Here, we investigate the electron–phonon interactions of nano-devices using two first-principles-based methods in numerically efficient manners. The first method is the Lowest Order Approximation (LOA) version of the computationally burdensome self-consistent Born approximation method. The LOA method incorporates the effect of each phonon mode on the electronic current perturbatively. In this work, we theoretically resolve the discrepancy between two conventional approaches of direct LOA calculation. To validate the correct approach, we compared its output with a completely different method (second method) named Special Thermal Displacement (STD) method. The STD method uses non-interacting transport calculation of the displaced atomic configuration of a device. We apply both methods to two thin-film nanodevices: 2D silicon junctionless FET and n-i-n FET. Both methods justify each other by providing similar results and exhibiting important quantum phenomena, such as phonon-assisted subthreshold swing degradation and tunneling.



## I. INTRODUCTION

As the nano-electronic devices get shorter and narrower, electronic transport exhibits significant quantum mechanical effects, such as quantum confinement[1] and tunneling.[2,3] Besides these effects, electron–phonon interactions remain significant even in nanoscale devices.[4–6] Accurate calculation of these effects has become a major challenge from the viewpoint of device simulations. The most difficult part of the calculation comes from the huge computational burden posed by the interactions between the electrons and the phonons. While the semiclassical transport theory failed to include quantum effects, the effective mass approximation also does not always ensure a correct calculation of the quantum effects. Deformation potentials (DPs) based Boltzmann transport equation (BTE) is quite suitable to calculate electron–phonon interactions for bulk materials.[7–12] However, it ignores phonon-assisted subthreshold swing degradation in nanoscale devices.[13] Therefore, the electronic properties of the nanodevices must be treated by the atomistic[14] quantum mechanical approach despite its computational burden.

Atomistic quantum mechanical calculations use non-equilibrium Green's function (NEGF) formalism along with either a semi-empirical tight-binding method or first-principles density functional theory (DFT). The advantage of the first-principles method is that it does not require to be fitted to a particular device. Luisier *et al.* have applied the self-consistent Born approximation (SCBA) algorithm using the NEGF formalism on a tight-binding basis to calculate electron–phonon scattering of Si nanowire

transistors.[15–18] Although it is computed with huge supercomputing resources, it failed to show phonon-assisted source-to-drain tunneling in the OFF-current state.

The electron–phonon interactions can be rigorously calculated by perturbation theory-based SCBA method using density functional theory (DFT). However, the computational burden limits its application to molecular-scale systems.[19,20] However, some approximations to the algorithm can unlock the scope of calculating electron–phonon scattering beyond molecular systems with modest computational resources. In this paper, we will investigate the approximation method called lowest order approximation (LOA).[21–26] The main difference between SCBA and LOA methods is that the SCBA method includes an infinite number of scattering diagrams, whereas the LOA method considers only the conserving diagrams.[26] The LOA method reduces the computational burden as it requires a much lesser number of iterations than SCBA to satisfy the conservation law. Hence, first order LOA needs the lowest computational cost as it requires only one iteration. Reference 23 shows that, in the weak-scattering regime, such as thin-film nanodevices, first order LOA is enough to show agreement with SCBA results. The LOA method considers the effect of each phonon mode perturbatively.

The LOA method can be implemented either by a direct algorithm[26] or by a rescaling technique.[25,26] The direct algorithm involves the Langreth theorem,[24,27] whereas the rescaling technique involves the Keldysh equation.[22,27–30] However, some articles implemented the LOA method with a direct algorithm using the Keldysh equation instead of the Langreth theorem.[20,31–35] In this article, we discuss the two conflicting approaches of the direct algorithm and theoretically resolve the issue.

A conceptually simple and efficient alternative to the perturbation theory-based LOA method is the stochastic sampling of lattice vibrations using Monte Carlo (MC)[36,37] or Molecular Dynamics (MD)[12] simulations. Recently, Zacharias *et al.*[36] found that a single supercell configuration can replace the stochastic sampling of lattice vibrations. Inspired by them, Gunst *et al.* presented a "special thermal displacement" (STD) method, which includes electron–phonon interaction by evaluating the first-principles Landauer–Büttiker transmission of configuration under a single displacement of the atoms.[13] Thus, the computational burden drastically reduces to the level of non-interacting calculations.

## II. METHODOLOGY

In this work, we investigate the electronic transport due to electron–phonon interactions using two first-principles-based approaches (LOA and STD). We apply these methods to two thin-film nanodevices: 2D silicon junctionless FET and n-i-n FET in order to validate the theoretical conclusion.

The steady-state electronic current from lead $\alpha = L, R$ to the central region including interactions in the device region can be represented as follows:[20,27,38,39]

$$\begin{aligned} \mathrm{I}_\alpha &= -2e\langle \dot{N}_\alpha \rangle = \frac{2e}{h}\int_{-\infty}^{\infty} d\varepsilon\ T_\alpha(\varepsilon), \\ T_\alpha(\varepsilon) &= Tr\{\Sigma_\alpha^<(\varepsilon)G^>(\varepsilon) - \Sigma_\alpha^>(\varepsilon)G^<(\varepsilon)\}, \end{aligned} \tag{1}$$

where $\dot{N}_\alpha = \sum_k c_{k\alpha}^\dagger c_{k\alpha}$ is an operator for electronic particle number, $T_\alpha(\varepsilon)$ is the transmission function, $\Sigma_\alpha^{\lessgtr}(\varepsilon)$ is the lesser/greater self-energy of lead $\alpha$, and $G^{\lessgtr}(\varepsilon)$ is the lesser/greater Green's function, incorporating all relevant interactions of the device region. The lesser/greater Green's function can be calculated from retarded Green's function ($G$) and advanced Green's function ($G^\dagger$) using the steady-state Keldysh equation,[27–30]

$$G^{\lessgtr} = G\left[\left(\sum_\alpha \Sigma_\alpha^{\lessgtr}\right) + \Sigma_{\mathrm{int}}^{\lessgtr}\right]G^\dagger, \tag{2}$$

where $\Sigma_{\mathrm{int}}$ and $\Sigma_{\mathrm{int}}^{\lessgtr}$ are the retarded and lesser/greater interaction self-energy, respectively, accounting for any interaction in the device region. In this paper, we will consider only electron–phonon interaction. Hence, interaction self-energy $\Sigma_{\mathrm{int}}$ can be represented as electron–phonon interaction self-energy $\Sigma_{ph}$. The retarded Green's function $G$ including electron–phonon interaction is given by the Dyson equation,[27–30]

$$G = g_0 + g_0\ \Sigma_{ph}[G]\ G, \tag{3}$$

where $g_0$ is the non-interacting retarded Green's function.

If no interactions in the device region are considered, we get $\Sigma_{int} = \Sigma_{int}^{\lessgtr} = 0$ and $G = g_0$, which turn Eq. (2) into

$$G^{\lessgtr} = g_0^{\lessgtr} = g_0\left[\sum_\alpha \Sigma_\alpha^{\lessgtr}\right]g_0^\dagger, \tag{4}$$

where $g_0^{\lessgtr}$ is the non-interacting lesser/greater Green's function. After some rewriting, Eq. (1) turns into the renowned Landauer–Büttiker formula for the non-interacting current,

$$\begin{aligned} I_0 &= \frac{2e}{h}\int_{-\infty}^{\infty} d\varepsilon\ T_0(\varepsilon)[f_L(\varepsilon) - f_R(\varepsilon)], \\ T_0(\varepsilon) &= \mathrm{Tr}\left\{\Gamma_L\ g_0\ \Gamma_R\ g_0^\dagger\right\}. \end{aligned} \tag{5}$$

To calculate current due to electron–phonon interaction, the electron–phonon interaction self-energy $\Sigma_{ph}$ should be calculated. We can represent interaction self-energies as[32,38,40]

$$\Sigma_{ph}^{\lessgtr}(\varepsilon) = \sum_\lambda i\int_{-\infty}^{\infty}\frac{d\omega_\lambda}{2\pi}M_\lambda\ D_0^{\lessgtr}(\omega_\lambda)\ \lambda\ G^{\lessgtr}(\varepsilon - \omega_\lambda)M_\lambda, \tag{6}$$

$$\Sigma_{ph} = \frac{1}{2}\left(\Sigma_{ph}^> - \Sigma_{ph}^<\right) - \frac{i}{2}\mathscr{H}\left(\Sigma_{ph}^> - \Sigma_{ph}^<\right), \tag{7}$$

where $M_\lambda$ represents electron–phonon coupling matrix for phonon mode $\lambda$, $\omega_\lambda$ are phonon frequencies, $D_0^{\lessgtr}$ is the lesser/greater free phonon Green's functions, and $\mathscr{H}$ is the Hilbert transform.

The solution of the Dyson equation [Eq. (3)] requires an iterative scheme with specific convergence criteria. Green's function at $N^{th}$ iteration can be assumed as $G_N \simeq G_{N-1}$, which leads to the representation of the Dyson equation as

$$G_N = \left[g_0^{-1} - \Sigma_{ph}[G_{N-1}]\right]^{-1}. \tag{8}$$

The Dyson equation [Eq. (8)] and Keldysh equation [Eq. (2)] along with Eqs. (6) and (7) can be solved iteratively to calculate the current including electron–phonon interaction. The scheme is called self-consistent Born approximation (SCBA), which is illustrated in Fig. 1.

Let us rewrite the Dyson equation [Eq. (8)] in the Taylor series expansion as

$$G_N = g_0 + g_0\Sigma[G_{N-1}]g_0 + g_0\Sigma[G_{N-1}]g_0\Sigma[G_{N-1}]g_0 + \cdots, \quad (9)$$

where $\Sigma_{ph}$ is written as $\Sigma$ for simplicity. From Eq. (9), the SCBA Green's function at first iteration $G_1$ is represented as

$$G_1 = g_0 + g_0\Sigma[g_0]g_0 + g_0\Sigma[g_0]g_0\Sigma[g_0]g_0 + \cdots. \quad (10)$$

The SCBA Green's function contains an infinite number of terms where some terms are currently conserving. The $G_1$ does not necessarily preserve the conservation law since there are higher-order non-conserving terms according to the corresponding scattering order.[22] The current conservation law is fulfilled when conserving terms are dominant over non-conserving ones. Therefore, a higher number of iterations may be required to fulfill the conservation law in the case of strong electron–phonon interactions, thereby increasing the computational cost.

If we calculate only the conserving terms in the SCBA Green's function, the current conservation law is satisfied at each scattering order. As only the lowest order conserving terms are considered, the method is called Lowest Order Approximation (LOA). The first-order LOA can be written as

$$G_{1LOA} = g_0 + g_0\Sigma[g_0]g_0, \quad (11)$$

where the interaction self-energy $\Sigma[g_0]$ is calculated only from the non-interacting Green's function $g_0$. Reference 23 showed that 1st order LOA is very similar to the SCBA in the weak-scattering regime. However, we can apply the Langreth theorem[24,27] to Eq. (12) to obtain the lesser/greater Green's function from the LOA Green's function directly,

$$G^{\lessgtr}_{1LOA} = g^{\lessgtr}_0 + g_0\Sigma[g_0]g^{\lessgtr}_0 + g_0\Sigma^{\lessgtr}[g_0]g^{\dagger}_0 + g^{\lessgtr}_0\Sigma^{\dagger}[g_0]g^{\dagger}_0. \quad (12)$$

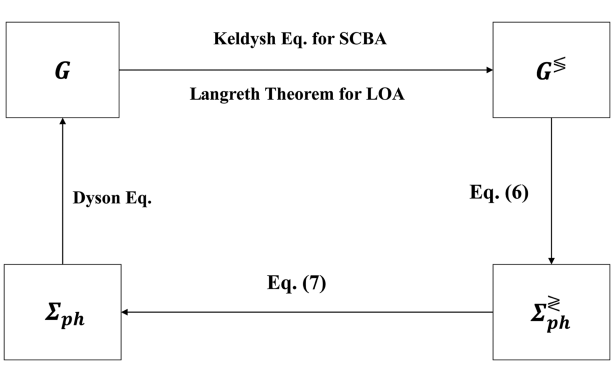


**FIG. 1.** Flow diagram of SCBA and LOA.

$\Sigma^{\lessgtr}[g_0]$ and $\Sigma[g_0]$ can be evaluated from Eqs. (6) and (7), respectively. $\Sigma^{\dagger}[g_0]$ denotes the advanced interaction self-energy.

However, in literature, some articles use an alternative approach to calculate directly the lesser/greater LOA Green's function, $G^{\lessgtr}_{LOA}$, from retarded Green's function, $G_{LOA}$, using Keldysh equation [Eq. (2)] instead of Langreth theorem.[20,31–35] However, this approach is shown here to be less accurate for the case of lowest order approximation. Keldysh equation can only be used to calculate lesser/greater Green's function from retarded Green's function for

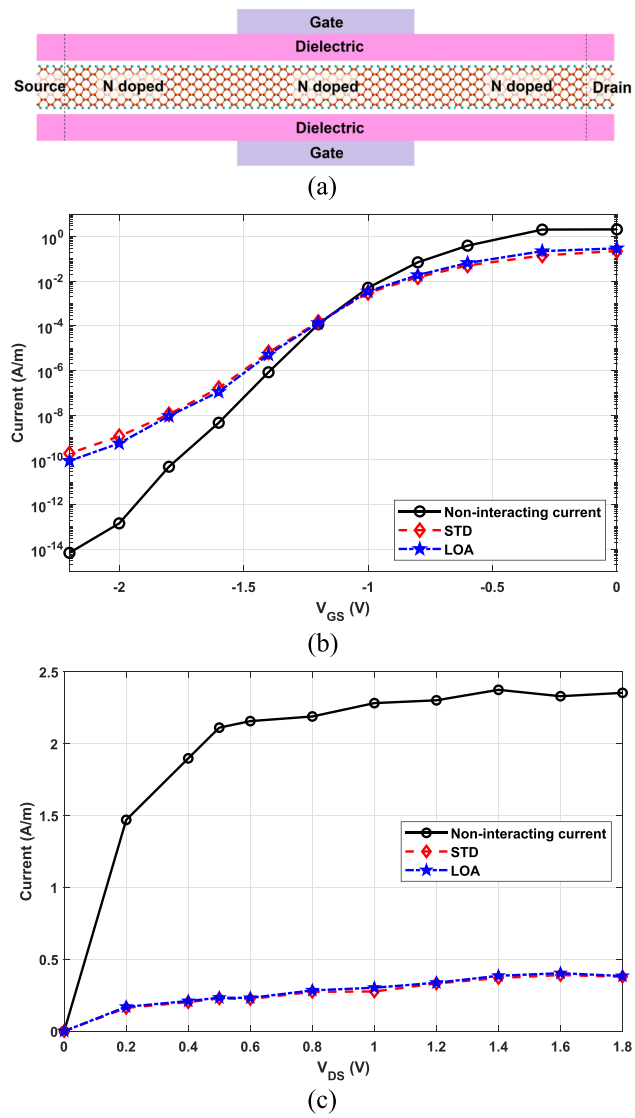


**FIG. 2.** (a) Junctionless silicon thin film FET with source, channel, and drain doping of $10^{20}$ cm$^{-3}$ (n-type) and ⟨100⟩ crystallographic orientation. The gate length $L_G$ = 7 nm, the source and drain length $L_{S/D}$ = 6.5 nm, and the thickness is 1.4 nm (total length is 20 nm with 740 atoms). (b) Current vs gate to source voltage, $V_{GS}$, for a drain-source voltage $V_{DS}$ = 0.05 V and at 300 K. (c) Current vs drain to source voltage, $V_{DS}$, for a gate-source voltage $V_{GS}$ = 0 V.

the case of self-consistent Born approximation. In the case of lowest order approximation if we use the Keldysh equation, we get

$$
\begin{aligned}
G^{\lessgtr}_{1LOA} &= G_{1LOA}\left[\sum_\alpha \Sigma^{\lessgtr}_\alpha + \Sigma^{\lessgtr}[g_0]\right] G^{\dagger}_{1LOA} \\
&= (g_0 + g_0\Sigma[g_0]g_0)\left[\sum_\alpha \Sigma^{\lessgtr}_\alpha + \Sigma^{\lessgtr}[g_0]\right]\left(g_0^{\dagger} + g_0^{\dagger}\Sigma^{\dagger}[g_0]g_0^{\dagger}\right) \\
&= g_0\left(\sum_\alpha \Sigma^{\lessgtr}_\alpha\right) g_0^{\dagger} + g_0\Sigma[g_0]g_0\left(\sum_\alpha \Sigma^{\lessgtr}_\alpha\right) g_0^{\dagger} + g_0\Sigma^{\lessgtr}[g_0]g_0^{\dagger} \\
&\quad + g_0\left(\sum_\alpha \Sigma^{\lessgtr}_\alpha\right) g_0^{\dagger}\Sigma^{\dagger}[g_0]g_0^{\dagger} + g_0\Sigma^{\lessgtr}[g_0]g_0^{\dagger}\Sigma^{\dagger}[g_0]g_0^{\dagger} \\
&\quad + g_0\Sigma[g_0]g_0\left(\sum_\alpha \Sigma^{\lessgtr}_\alpha\right) g_0^{\dagger}\Sigma^{\dagger}[g_0]g_0^{\dagger} \\
&\quad + g_0\Sigma[g_0]g_0\Sigma^{\lessgtr}[g_0]\left(g_0^{\dagger} + g_0^{\dagger}\Sigma^{\dagger}[g_0]g_0^{\dagger}\right) \\
&= g_0^{\lessgtr} + g_0\Sigma[g_0]g_0^{\lessgtr} + g_0\Sigma^{\lessgtr}[g_0]g_0^{\dagger} + g_0^{\lessgtr}\Sigma^{\dagger}[g_0]g_0^{\dagger} \\
&\quad + g_0\Sigma^{\lessgtr}[g_0]g_0^{\dagger}\Sigma^{\dagger}[g_0]g_0^{\dagger} + g_0\Sigma[g_0]g_0^{\lessgtr}\Sigma^{\dagger}[g_0]g_0^{\dagger} \\
&\quad + g_0\Sigma[g_0]g_0\Sigma^{\lessgtr}[g_0]\left(g_0^{\dagger} + g_0^{\dagger}\Sigma^{\dagger}[g_0]g_0^{\dagger}\right),
\end{aligned}
\tag{13}
$$

where $g_0^{\lessgtr} = g_0\left[\sum_\alpha \Sigma^{\lessgtr}_\alpha\right]g_0^{\dagger}$ [Eq. (4)]. Here, the first four terms of Eq. (14) are similar to that of Eq. (13). The last three terms of Eq. (13) are redundant and will cause incorrect results. Therefore, the Keldysh equation is not suitable for calculating lesser/greater Green's function for the case of lowest order approximation. To get a more correct LOA current, we need to use $G^{\lessgtr}_{1LOA}$ calculated in Eq. (12) instead of Eq. (13). Here, we finally get the interacting current equation by substituting $G^{\lessgtr}(\varepsilon)$ with $G^{\lessgtr}_{1LOA}$ in Eq. (1),

$$
\begin{aligned}
I_\alpha = \frac{2e}{h}\int_{-\infty}^{\infty} d\varepsilon\, Tr\Big[&\Sigma^{<}_\alpha(\varepsilon)\left\{g_0^{>} + g_0\Sigma[g_0]g_0^{>} + g_0\Sigma^{>}[g_0]g_0^{\dagger}\right. \\
&\left. + g_0^{>}\Sigma^{\dagger}[g_0]g_0^{\dagger}\right\} - \Sigma^{>}_\alpha(\varepsilon)\left\{g_0^{<} + g_0\Sigma[g_0]g_0^{<}\right. \\
&\left. + g_0\Sigma^{<}[g_0]g_0^{\dagger} + g_0^{<}\Sigma^{\dagger}[g_0]g_0^{\dagger}\right\}\Big].
\end{aligned}
\tag{14}
$$

The first-principles calculation of LOA current can be computationally burdensome for large devices. The main computational burden comes from the first-principles calculation of the electron–phonon coupling matrix $M_\lambda$ and its integration over a large number of phonon modes $\lambda$ (e.g., 3000 phonon modes for a device of 1000 atoms). The coupling matrix is calculated from the dynamical matrix and Hamiltonian derivates. The computational burden of Dynamical matrix calculation can be reduced significantly by using classical force-field calculation using Tersoff potential.[41] In repeated two-probe devices, where the atomic configuration of the central region is a repetition of the electrode unit cell along the transport direction, Hamiltonian derivates of the central region

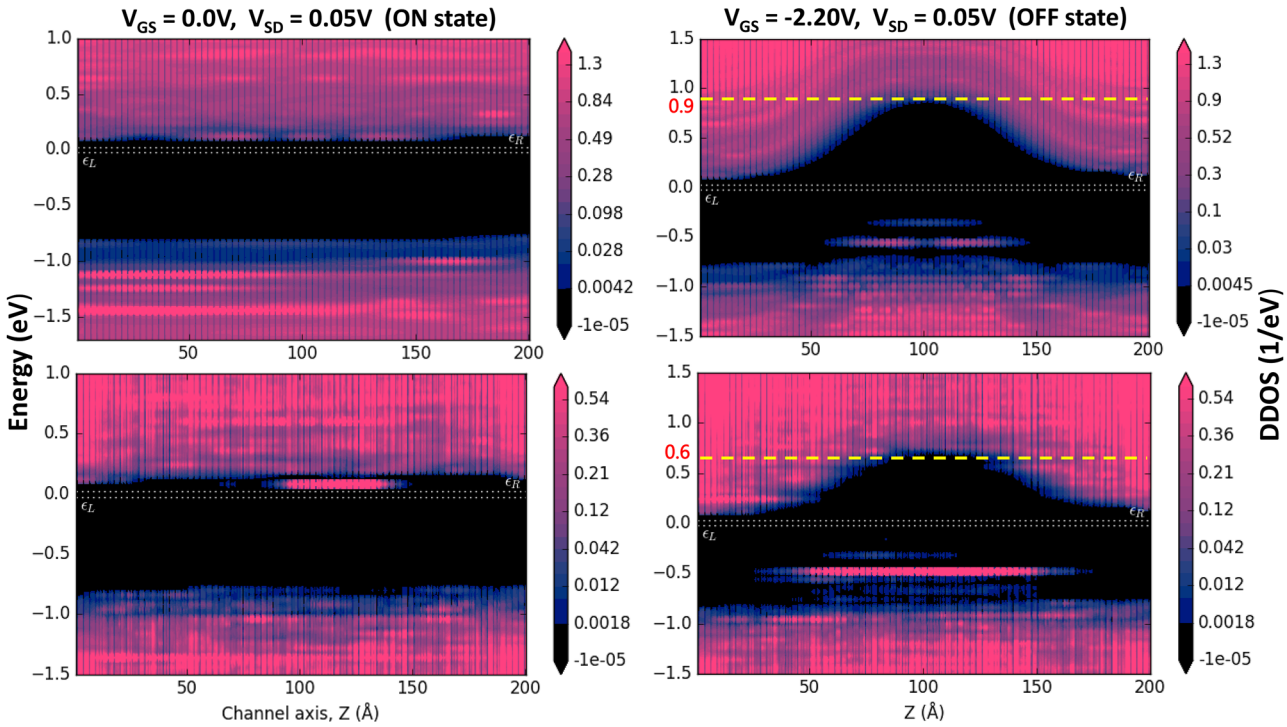


**FIG. 3.** Projected local device density of states (DDOS) of junctionless FET shows little change between non-interacting and interacting devices in the ON state, but the OFF state shows a decrease in the conduction band edge (from 0.9 to 0.6 eV) in the channel region due to electron–phonon interaction. $\varepsilon_L$ and $\varepsilon_R$ denote the left and right electrode Fermi levels.

can be approximated from that of the electrode unit cell. Additionally, instead of using a large number of phonon modes, we can sum the phonon modes in energy intervals to create new effective phonon modes. The sufficient number of effective phonon modes is usually less than 50, which further reduces the computation cost.

An alternative way to include electron–phonon interaction on current is the stochastic sampling of lattice vibrations. However, when stochastic sampling with these methods is performed, many transmission calculations must be done with increasing computational cost. Recently, Zacharias *et al.*[36] discovered that a single supercell configuration is representative of all the samples of lattice vibrations. Calculating the non-interacting Landauer–Büttiker transmission $T_0$ of that single lattice configuration is enough to obtain interacting current. The method is known as Special Thermal Displacement (STD) method.[13] The interacting current due to electron–phonon interaction can be calculated as the thermally averaged current for atomic displacements, $u_\lambda(T, V)$, given by[13]

$$I(V,T) = \frac{2e}{h}\int dE\langle\mathcal{T}(E,T)\rangle[f_L - f_R],$$
$$\langle\mathcal{T}(E,T)\rangle = \Pi_\lambda \int du_\lambda \frac{\exp(-u_\lambda^2/2\sigma_\lambda^2)}{\sqrt{2\pi\sigma_\lambda}}\langle\mathcal{T}(E,\{u_\lambda\})\rangle. \tag{15}$$

According to Ref. 13, sampling of displacements, $u_\lambda(T, V)$, can be replaced by a single displacement given by

$$u_{STD}(T) = \sum_\lambda s_\lambda(-1)^{\lambda-1}\sigma_\lambda(T)\mathbf{e}_\lambda. \tag{16}$$

If we compare the Tailor expansion of Eq. (15) around $u_\lambda$ with Taylor expansion around $u_{STD}$, both expressions tend to be the same for large systems. Because in large systems, for each pair of degenerate phonon modes, the corresponding terms of the Taylor series cancel each other, resulting in only the even-order terms, which are similar for both Taylor series. Thus, the STD configuration approximates the correct thermally averaged current.

## III. RESULTS

The first device we investigate for electron–phonon interaction is a 2D silicon junctionless double-gated FET with a 7 nm gate length [Fig. 2(a)]. The electronic transport occurs along the ⟨100⟩ crystallographic direction (horizontal direction) under the quantum confinements in the vertical direction. The surfaces of 2D silicon structure in a confined direction are passivated with Hydrogen atoms, and the out-of-plane direction is periodic. Two 1 nm-thick $SiO_2$ dielectric layers surround the silicon structure in confined directions. The device has the same n-type doping in the source, channel, and drain region. That is why it is called junctionless FET due to no junction in the transport direction.

In the first principles calculation (DFT), we use Local Density Approximation (LDA) in combination with norm-conserving pseudopotentials. We use a single-zeta-polarized basis set for Si and H atoms along with 9 k-points in the periodic direction and 87 k-points in the transport direction. In order to calculate electron–phonon interaction either by LOA method or by STD method, we need a Dynamical matrix, which is calculated from classical force-field calculation using Tersoff potential.[41]

In the current vs gate voltage characteristics graph [Fig. 2(b)], the comparison between non-interacting currents and interacting currents (calculated by LOA and STD method) is shown. We observe that electron–phonon interaction has more and opposite effect in the OFF-current than ON-current. This phenomenon can be explained by the scattering and tunneling effect. In the ON-current state, electron–phonon scattering is dominant but not too strong due to the very short channel length. That is why, ON-current is reduced due to electron–phonon interaction, but the reduction is not too

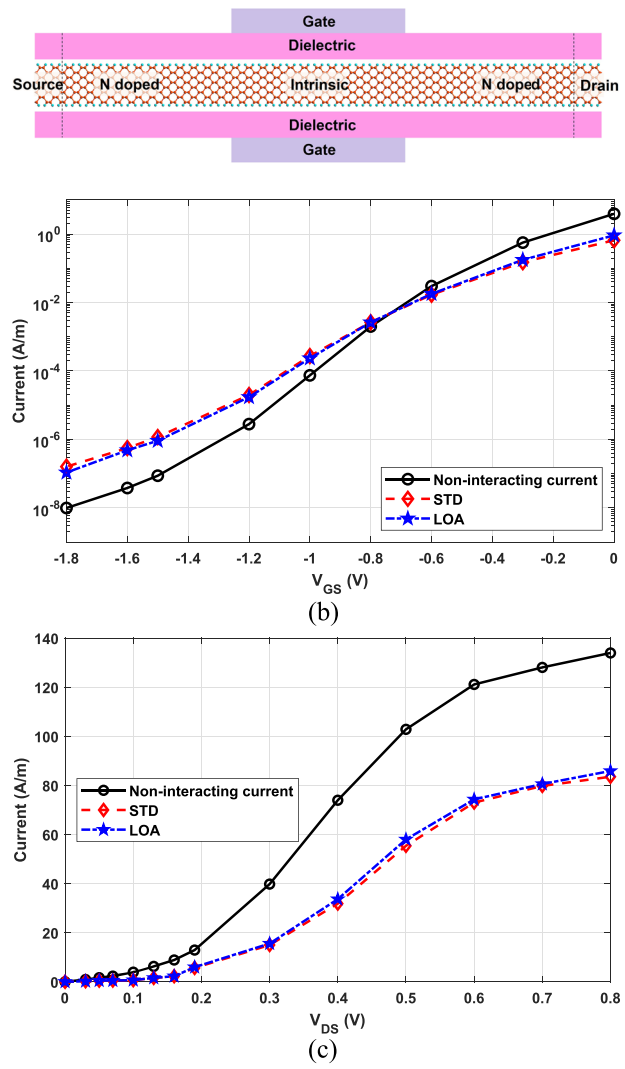


**FIG. 4.** (a) n-i-n silicon thin film FET with source and drain doping of $10^{21}$ cm$^{-3}$ and ⟨100⟩ crystallographic orientation. The gate length $L_G$ = 7 nm, the source and drain length $L_{S/D}$ = 6.5 nm, and the thickness is 1.4 nm (total length is 20 nm with 740 atoms). (b) Current vs gate to source voltage, $V_{GS}$, for a source–drain voltage $V_{SD}$ = 0.1 V and at 300 K. (c) Current vs drain to source voltage, $V_{DS}$, for a gate-source voltage $V_{GS}$ = 0 V.

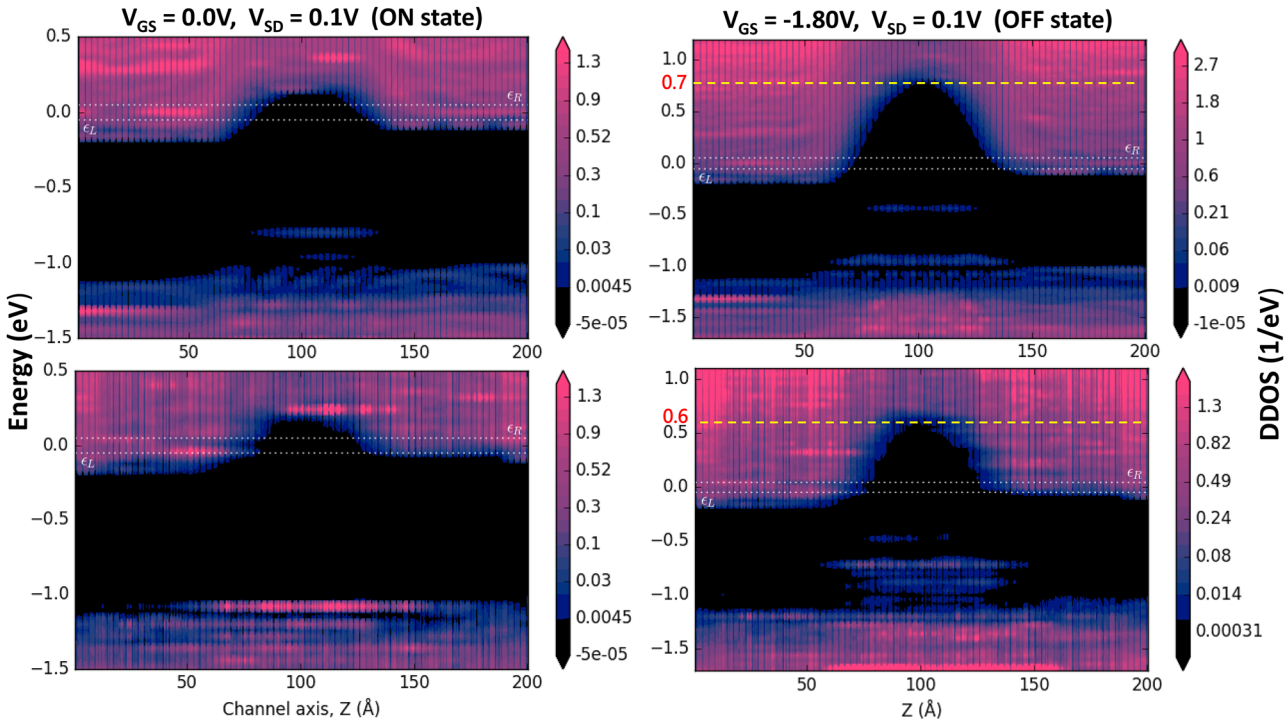


**FIG. 5.** Projected local device density of states (DDOS) of n-i-n FET shows little change between non-interacting and interacting devices in the ON state, but the OFF state shows a decrease in the conduction band edge (from 0.7 to 0.6 eV) in the channel region due to electron–phonon interaction. $\varepsilon_L$ and $\varepsilon_R$ denote the left and right electrode Fermi levels.

high. In the OFF-current state, the tunneling effect is much greater than the scattering effect. This leads to an increase in OFF-current up to four orders of magnitude and degradation of subthreshold slope from 100 to 150 mV/dec.

Figure 2(c) shows the current vs drain voltage characteristics for non-interacting and interacting cases. The ON-current reduction is due to the electron–phonon scattering effect. In Figs. 2(b) and 2(c), the interacting currents obtained by LOA and STD methods show excellent agreement. Since the two methods are very different, it can be perceived that these two approaches for interacting with current calculation are valid.

The projected local device density of states of the junctionless FET in Fig. 3 shows little change in the ON current stage due to electron–phonon interaction, which supports the low ON-current reduction. In the OFF-current stage, a considerable decrease in the conduction band edge (from 0.9 to 0.6 eV) in the channel region is shown. The decrease of the conduction band edge indicates the large increase of OFF-current due to electron–phonon interaction.

The second device under investigation is similar to the first device except for the doping profile. It is a two-dimensional silicon n-i-n double-gated FET with a 7 nm gate length [Fig. 4(a)]. Unlike junctionless FET, this device has an intrinsic silicon region under the gates and an n-doping region outside the gate. The n-type doping of $10^{21}$ $cm^{-3}$ is ten times of the junctionless case. The electronic transport in this device occurs along the ⟨100⟩ crystallographic direction (horizontal direction) under the quantum confinements in the vertical direction similar to the junctionless FET. The hydrogen passivation and dielectric layers of this device are the same as the first device. The first-principles calculation and classical force field calculation of the n-i-n FET are the same as the junctionless FET.

Figure 4(b) shows the interacting and non-interacting current vs gate voltage of the n-i-n FET. The interacting current is calculated by LOA and STD methods. The ON-current reduction and OFF-current increase due to electron–phonon interaction follow the trend of the junctionless device. The explanation for the change in current is same as for the first device. However, n-i-n FET has a lower OFF-current increase than the junctionless device. The OFF-current is increased up to ten times, and the subthreshold slope is degraded from 150 to 185 mV/dec due to electron–phonon interaction.

**TABLE I.** Comparison among different parameters of the two devices.

| Devices | Increase in OFF-current | Degradation in subthreshold slope (mV/dec) | Decrease in conduction bandedge (eV) |
|---|---|---|---|
| Junctionless FET | $10^4$ | 100 to 150 | 0.9 to 0.6 |
| n-i-n FET | $10^1$ | 150 to 185 | 0.7 to 0.6 |

**TABLE II.** Comparison between proposed and conventional method[42] in terms of computational time.

| | Proposed LOA method (for a device consisting of 740 atoms) | Conventional LOA (for a device consisting of only 56 atoms) |
|---|---|---|
| Time spent on IV curve (in terms of core hours) | 90 h | 468 h |

Figure 4(c) shows the current vs drain voltage characteristics for non-interacting and interacting cases. The ON-current is reduced due to the electron–phonon interaction. Again, in this n-i-in FET, the interacting currents calculated by LOA and STD methods show excellent agreement, which reconfirms that the two methods for interacting current calculation are valid.

The projected local device density of states of the n-i-in FET in Fig. 5 shows little change in the ON current stage due to electron–phonon interaction, which supports the low ON-current reduction. In the OFF-current stage, a decrease in the conduction band edge (from 0.7 to 0.6 eV) in the channel region is shown. The decrease of the conduction band edge indicates the increase of OFF-current due to electron–phonon interaction.

Table I presents the comparison among the various parameters of junctionless FET and n-i-in FET. The junctionless device seems to have a greater change in parameters due to electron–phonon interaction.

Table II presents the comparison between our proposed LOA method and a conventional LOA method[42] in terms of computational time required for the IV curve. The conventional LOA method requires higher time for simulating a device of only 56 atoms, whereas our device consists of 740 atoms and still requires lesser time using our proposed method.

## IV. CONCLUSION

In summary, we have made several approximations on the LOA method, such as classical force-field calculation of dynamical matrix, a small number of effective phonon modes, and coupling matrix calculation of repeatable electrode unit cell. These pave the way for calculating electron–phonon interaction with modest computational resources. Among the two existing approaches of the direct LOA method, the Langreth theorem-based approach is theoretically shown to be accurate. To validate the approach, we have compared the output of the LOA method with that of the STD method. The STD method does not require the burdensome calculation of electron–phonon coupling matrix and thereby reduces the computational cost greatly. We have demonstrated phonon-limited electronic transport for junctionless FET and n-i-in FET using the two first-principles methods. As both devices maintain low electron–phonon scattering, 1st LOA is shown to be sufficient to give accurate results. Both methods show a similar decrease in ON-current, increase in OFF-current, and degradation of subthreshold slope in the two devices. Since the two very different methods provide similar outputs for both devices, it confirms that the two methods for interacting current calculation are justified. The computational strategy of the STD method makes it appealing for device modeling where the LOA method may not work due to strong electron–phonon scattering.

## AUTHOR DECLARATIONS

### Conflict of Interest

The authors have no conflicts to disclose.

### Author Contributions

**Md. Samzid Bin Hafiz**: Conceptualization (lead); Data curation (lead); Formal analysis (lead); Investigation (lead); Methodology (lead); Software (lead); Validation (lead); Visualization (lead). **Quazi Deen Mohd Khosru**: Supervision (lead); Writing – original draft (supporting). **Momotaz Begum**: Formal analysis (supporting); Investigation (supporting). **Bimal Chandra Das**: Formal analysis (supporting); Investigation (supporting).

## DATA AVAILABILITY

The data that support the findings of this study are available from the corresponding author upon reasonable request.

## REFERENCES

[1] X. Zhao, C. M. Wei, L. Yang, and M. Y. Chou, "Quantum confinement and electronic properties of silicon nanowires," Phys. Rev. Lett. **92**, 236805 (2004).
[2] M. Moussavou, N. Cavassilas, E. Dib, and M. Bescond, "Influence of uniaxial strain in Si and Ge p-type double-gate metal-oxide-semiconductor field effect transistors," J. Appl. Phys. **118**, 114503 (2015).
[3] G. Pizzi, M. Gibertini, E. Dib, N. Marzari, G. Iannaccone, and G. Fiori, "Performance of arsenene and antimonene double-gate MOSFETS from first principles," Nature Commun. **7**, 12585 (2016).
[4] J. Cao, D. Logoteta, S. Özkaya, B. Biel, A. Cresti, M. G. Pala, and D. Esseni, "Operation and design of van der waals tunnel transistors: A 3-D quantum transport study," IEEE Trans. Electron Devices **63**, 4388–4394 (2016).
[5] F. Murphy-Armando, G. Fagas, and J. C. Greer, "Deformation potentials and electron–phonon coupling in silicon nanowires," Nano Lett. **10**, 869–873 (2010).
[6] S. D. Suk, M. Li, Y. Y. Yeoh, K. H. Yeo, K. H. Cho, I. K. Ku, H. Cho, W. Jang, D.-W. Kim, D. Park *et al.*, "Investigation of nanowire size dependency on TSNWFET," in *2007 IEEE International Electron Devices Meeting* (IEEE, 2007), pp. 891–894.
[7] T. Gunst, T. Markussen, K. Stokbro, and M. Brandbyge, "First-principles method for electron-phonon coupling and electron mobility: Applications to two-dimensional materials," Phys. Rev. B **93**, 035414 (2016).
[8] F. Giustino, "Electron-phonon interactions from first principles," Rev. Mod. Phys. **89**, 015003 (2017).
[9] K. Kaasbjerg, K. S. Thygesen, and K. W. Jacobsen, "Unraveling the acoustic electron-phonon interaction in graphene," Phys. Rev. B **85**, 165440 (2012).
[10] C.-H. Park, N. Bonini, T. Sohier, G. Samsonidze, B. Kozinsky, M. Calandra, F. Mauri, and N. Marzari, "Electron–phonon interactions and the intrinsic electrical resistivity of graphene," Nano Lett. **14**, 1113–1119 (2014).
[11] E. H. Hwang and S. Das Sarma, "Acoustic phonon scattering limited carrier mobility in two-dimensional extrinsic graphene," Phys. Rev. B **77**, 115449 (2008).
[12] T. Markussen, M. Palsgaard, D. Stradi, T. Gunst, M. Brandbyge, and K. Stokbro, "Electron-phonon scattering from green's function transport

combined with molecular dynamics: Applications to mobility predictions," Phys. Rev. B **95**, 245210 (2017).
[13]T. Gunst, T. Markussen, M. L. N. Palsgaard, K. Stokbro, and M. Brandbyge, "First-principles electron transport with phonon coupling: Large scale at low cost," Phys. Rev. B **96**, 161404 (2017).
[14]M. Luisier, A. Schenk, and W. Fichtner, "Full-band atomistic study of source-to-drain tunneling in Si nanowire transistors," *Simulation of Semiconductor Processes and Devices 2007* (Springer, 2007), pp. 221–224.
[15]M. Luisier and G. Klimeck, "Atomistic full-band simulations of silicon nanowire transistors: Effects of electron-phonon scattering," Phys. Rev. B **80**, 155430 (2009).
[16]M. Luisier, "Phonon-limited and effective low-field mobility in *n*-and *p*-type [100]-,[110]-, and [111]-oriented si nanowire transistors," Appl. Phys. Lett. **98**, 032111 (2011).
[17]M. Luisier, "Performance comparison of GaSb, strained-Si, and InGaAs double-gate ultrathin-body n-FETS," IEEE Electron Device Lett. **32**, 1686–1688 (2011).
[18]M. Luisier, R. Rhyner, A. Szabo, and A. Pedersen, "Atomistic simulation of nanodevices," in *2016 International Conference on Simulation of Semiconductor Processes and Devices (SISPAD)* (IEEE, 2016), pp. 281–286.
[19]T. Frederiksen, M. Brandbyge, N. Lorente, and A.-P. Jauho, "Inelastic scattering and local heating in atomic gold wires," Phys. Rev. Lett. **93**, 256601 (2004).
[20]T. Frederiksen, M. Paulsson, M. Brandbyge, and A.-P. Jauho, "Inelastic transport theory from first principles: Methodology and application to nanoscale devices," Phys. Rev. B **75**, 205413 (2007).
[21]H. Mera, M. Lannoo, C. Li, N. Cavassilas, and M. Bescond, "Inelastic scattering in nanoscale devices: One-shot current-conserving lowest-order approximation," Phys. Rev. B **86**, 161404 (2012).
[22]H. Mera, M. Lannoo, N. Cavassilas, and M. Bescond, "Nanoscale device modeling using a conserving analytic continuation technique," Phys. Rev. B **88**, 075147 (2013).
[23]N. Cavassilas, M. Bescond, H. Mera, and M. Lannoo, "One-shot current conserving quantum transport modeling of phonon scattering in n-type double-gate field-effect-transistors," Appl. Phys. Lett. **102**, 013508 (2013).
[24]Y. Lee, M. Lannoo, N. Cavassilas, M. Luisier, and M. Bescond, "Efficient quantum modeling of inelastic interactions in nanodevices," Phys. Rev. B **93**, 205411 (2016).
[25]Y. Lee, M. Bescond, N. Cavassilas, D. Logoteta, L. Raymond, M. Lannoo, and M. Luisier, "Quantum treatment of phonon scattering for modeling of three-dimensional atomistic transport," Phys. Rev. B **95**, 201412 (2017).
[26]Y. Lee, D. Logoteta, N. Cavassilas, M. Lannoo, M. Luisier, and M. Bescond, "Quantum treatment of inelastic interactions for the modeling of nanowire field-effect transistors," Materials **13**, 60 (2020).
[27]H. Haug, A.-P. Jauho *et al.*, *Quantum Kinetics in Transport and Optics of Semiconductors* (Springer, 2008), Vol. 2.
[28]L. V. Keldysh *et al.*, "Diagram technique for nonequilibrium processes," Sov. Phys. JETP **20**, 1018–1026 (1965).
[29]R. A. Craig, "Perturbation expansion for real-time Green's functions," J. Math. Phys. **9**, 605–611 (1968).
[30]P. Danielewicz, "Quantum theory of nonequilibrium processes, I," Ann. Phys. **152**, 239–304 (1984).
[31]J. K. Viljas, J. C. Cuevas, F. Pauly, and M. Häfner, "Electron-vibration interaction in transport through atomic gold wires," Phys. Rev. B **72**, 245415 (2005).
[32]M. Paulsson, T. Frederiksen, and M. Brandbyge, "Modeling inelastic phonon scattering in atomic-and molecular-wire junctions," Phys. Rev. B **72**, 201101 (2005).
[33]W. Vandenberghe, B. Sorée, W. Magnus, and M. V. Fischetti, "Generalized phonon-assisted zener tunneling in indirect semiconductors with non-uniform electric fields: A rigorous approach," J. Appl. Phys. **109**, 124503 (2011).
[34]Y. Zhang, C. Y. Yam, and G. Chen, "Dissipative time-dependent quantum transport theory," J. Chem. Phys. **138**, 164121 (2013).
[35]J.-T. Lü, R. B. Christensen, G. Foti, T. Frederiksen, T. Gunst, and M. Brandbyge, "Efficient calculation of inelastic vibration signals in electron transport: Beyond the wide-band approximation," Phys. Rev. B **89**, 081405 (2014).
[36]M. Zacharias, C. E. Patrick, and F. Giustino, "Stochastic approach to phonon-assisted optical absorption," Phys. Rev. Lett. **115**, 177401 (2015).
[37]B. Monserrat, "Vibrational averages along thermal lines," Phys. Rev. B **93**, 014302 (2016).
[38]T. Frederiksen, "Inelastic electron transport in nanosystems," Master's thesis, Technical University of Denmark, 2004.
[39]Y. Meir and N. S. Wingreen, "Landauer formula for the current through an interacting electron region," Phys. Rev. Lett. **68**, 2512 (1992).
[40]M. Palsgaard, M. Brandbyge, T. Gunst, T. Markussen, A. Jauho, and D. Rideau, "Bridging first principles modelling with nanodevice TCAD simulations," Ph.D. thesis, Technical University of Denmark, 2018.
[41]J. Tersoff, "Empirical interatomic potential for silicon with improved elastic properties," Phys. Rev. B **38**, 9902 (1988).
[42]See https://docs.quantumatk.com/casestudies/std_transport/std_transport.html#std-transport for more information about a conventional LOA method.